UNIVERSITY of York

This is a repository copy of *Statistical analysis of the dynamic behavior of individual discharges during the ignition and continuous phases of contact glow discharge electrolysis*.

White Rose Research Online URL for this paper:
https://eprints.whiterose.ac.uk/226911/

Version: Published Version

---

**Article:**
Forschner, Lukas, Gembus, Jan Luca, Schücke, Lars et al. (4 more authors) (2025) Statistical analysis of the dynamic behavior of individual discharges during the ignition and continuous phases of contact glow discharge electrolysis. Journal of Physics D: Applied Physics. 215204. ISSN 0022-3727

https://doi.org/10.1088/1361-6463/adce16

---

**Reuse**
This article is distributed under the terms of the Creative Commons Attribution (CC BY) licence. This licence allows you to distribute, remix, tweak, and build upon the work, even commercially, as long as you credit the authors for the original work. More information and the full terms of the licence here: https://creativecommons.org/licenses/

**Takedown**
If you consider content in White Rose Research Online to be in breach of UK law, please notify us by emailing eprints@whiterose.ac.uk including the URL of the record and the reason for the withdrawal request.

White Rose university consortium
Universities of Leeds, Sheffield & York

eprints@whiterose.ac.uk
https://eprints.whiterose.ac.uk/

Journal of Physics D:
Applied Physics

PURPOSE-LED PUBLISHING™

**PAPER** • **OPEN ACCESS**

# Statistical analysis of the dynamic behavior of individual discharges during the ignition and continuous phases of contact glow discharge electrolysis

To cite this article: Lukas Forschner *et al* 2025 *J. Phys. D: Appl. Phys.* **58** 215204

View the article online for updates and enhancements.

You may also like

- Vapor Drainage in the Protolunar Disk as the Cause for the Depletion in Volatile Elements of the Moon
Nicole X. Nie and Nicolas Dauphas
- Cavity formation during water entry of heated spheres
Jia-Chuan Li, , Ying-Jie Wei et al.
- Drag reduction characteristics of heated spheres falling into water
Jia-Chuan Li, , Ying-Jie Wei et al.


This content was downloaded from IP address 144.32.224.27 on 20/05/2025 at 15:51

OPEN ACCESS
IOP Publishing
Journal of Physics D: Applied Physics
J. Phys. D: Appl. Phys. **58** (2025) 215204 (11pp)
https://doi.org/10.1088/1361-6463/adce16

# Statistical analysis of the dynamic behavior of individual discharges during the ignition and continuous phases of contact glow discharge electrolysis

**Lukas Forschner[1], Jan-Luca Gembus[2], Lars Schücke[2], Peter Awakowicz[2], Andrew R Gibson[2,3], Timo Jacob[1,*] and Albert K Engstfeld[1,*]**

[1] Institute of Electrochemistry, Ulm University, D-89081 Ulm, Germany
[2] Chair of Applied Electrodynamics and Plasma Technology, Ruhr University Bochum, D-44801 Bochum, Germany
[3] York Plasma Institute, School of Physics, Engineering and Technology, University of York, Heslington UK-YO10 5DD, United Kingdom

E-mail: timo.jacob@uni-ulm.de and albert.engstfeld@uni-ulm.de

Received 3 February 2025, revised 14 April 2025
Accepted for publication 17 April 2025
Published 7 May 2025

**Abstract**

Contact Glow Discharge Electrolysis (CGDE) denotes a plasma inside a vapor layer surrounding a gas-evolving electrode immersed in an aqueous electrolyte and operated at high voltages. We used a high-speed camera to image the formation of the vapor layer as well as its dynamic behavior during continuous CGDE on a Au wire cathode. The plasma ignites with a spark within a large bubble at the tip, which expands along the wire to the top, leaving a stable glow within the vapor layer behind. Using an in-house developed open-source Python-based software we deduced, from a thorough statistical analysis of images taken during continuous CGDE, a vapor layer thickness between 0.1 and 0.4 mm. Furthermore, we provide information on the dynamic behavior of individual discharges through the vapor layer from a series of images. The discharges are confined within the vapor layer and, thus, the extent of the discharges is similar to the vapor layer thickness. We find that the discharges have approximately the shape of oblate spheroids, which appear either as circles or ellipses in the camera images, depending on the orientation of the discharge with respect to the camera. We discuss the relevance of our results for the fundamental understanding of atomic scale surface structural changes and products formed in the solution in the presence of the plasma.

Supplementary material for this article is available online

Keywords: contact glow discharge analysis, discharge dynamics, plasma, electrolysis

* Authors to whom any correspondence should be addressed.

Original Content from this work may be used under the terms of the Creative Commons Attribution 4.0 licence. Any further distribution of this work must maintain attribution to the author(s) and the title of the work, journal citation and DOI.


© 2025 The Author(s). Published by IOP Publishing Ltd

## 1. Introduction

Continuously glowing plasmas in solution can be obtained by applying a sufficiently high voltage (DC) between two gas-evolving electrodes of different sizes in an electrolyte, where the plasma is confined within a vapor layer surrounding the smaller electrode. While the effect was already observed in the middle of the 19th century [1, 2], the first systematic studies in aqueous solutions only appeared in the middle of the 20th century [3, 4]. Today, this process is commonly denoted as Contact Glow Discharge Electrolysis (CGDE) or Plasma Electrolysis.

The interest in plasmas in contact with liquids in general [5–8], and CGDE specifically, has increased over the past decades, where the technique has been discussed for possible applications such as synthetic chemistry [9, 10], wastewater treatment [6, 11–13], surface modification [14–17], or nanoparticle formation [5, 18, 19]. The processes during CGDE depend on the polarity of the driving electrode. Generally, during normal electrolysis (lower voltages) in aqueous electrolytes, $O_2$ forms at the anode via the oxygen evolution reaction and $H_2$ at the cathode via the hydrogen evolution reaction. During anodic CGDE, in addition to $O_2$, the formation of $H_2$, $H_2O_2$, and other reaction intermediates (including radicals, ions, etc) was also observed [20]. Species such as $H_2O_2$ were found to be crucial for the degradation of organic molecules during CGDE [12, 21] or the modification of electrode surfaces after CGDE [16, 22]. Cathodic CGDE has proven to be a versatile approach for nanoparticle synthesis, either from ions within the electrolyte or by decomposing the electrode material [5, 18, 19]. Aside from the polarity, the color of the plasma emission depends on the composition of the electrode and electrolyte [4, 23, 24].

Over the last decades, many studies have aimed to gain more fundamental insights into the reasons for the observed phenomena, e.g. emission color, product formation, or material modification. An early work by Kellogg provides the first images of the vapor layer engulfing the electrode during anodic CGDE [3]. Further studies provided additional insights into the physical properties of the gas evolution on electrodes at high current densities during normal electrolysis at high voltages [25–27] as well as the transition to CGDE during voltage increase [28–32]. These studies clearly illustrate that during CGDE, the electrode is isolated from the electrolyte by a vapor layer, which increases the interfacial resistance, and the current flows through the plasma ignited in this phase. Several works provide information on the plasma's properties during CGDE, using mostly optical emission spectroscopy. Limited studies, however, provide direct visual insights into the plasma within the vapor layer [23, 24, 33–37].

Following, we provide a brief overview of studies using electrodes of various shapes. For example, Schaper *et al* used shadowgraphic imaging to study the plasma ignition on a millisecond timescale for different voltages at a W rod cathode (0.5 mm diameter and 0.5 mm long) with 0.9% NaCl in distilled water. For low voltages, individual localized sparks were observed, whereas at high voltages, the plasma covered the entire electrode. The authors denoted the observed plasma as micro-arc discharges [33, 34]. A longer Pt wire electrode (10 mm long, 0.5 mm diameter, and protected tip) was investigated in NaOH solutions by Saito *et al* using high-speed camera imaging, revealing individual sparks for low voltages and continuous plasma for higher voltages [35]. For a wire without tip protection, a different type of discharge was observed at the unprotected side. The same group also studied flat plate electrodes of different metals (Au, Ni, Ti, and Zn), showing a continuous glow discharge during cathodic CGDE, whose color depended on the metal substrate, indicating the presence of ions from the substrate in the plasma phase [24]. From high-speed camera images, a non-uniform distribution of individual sparks was observed on the electrode surface. Both Stojadinović *et al* [36] and Yerokhin *et al* [37] showed for cathodic and anodic CGDE, respectively, that when using metal sheet electrodes, plasma emission is preferentially located at the edge of the electrode.

Previous studies have been limited in discussing observations from selected images of the vapor layer and/or the discharge emission. This work aims to provide a statistical analysis of discharges observed in individual frames, and also during a series of frames, which will help to gain more fundamental insights into atomic scale processes at the electrode surface, in the plasma, and at the different interfaces.

To demonstrate our analytical approach, we study Au wire electrodes immersed in an alkaline KOH electrolyte during cathodic CGDE, using high-speed camera imaging with and without background illumination. The images were evaluated using an open-source software package developed in-house based on Python [38]. We discuss multiple aspects, such as the shape, size, distribution, and velocity of the discharges in the vapor layer, as well as the vapor layer itself, from a qualitative and quantitative evaluation of the images to the recorded currents. We also provide additional information on the ignition process of cathodic CGDE on wire electrodes.

## 2. Experimental

### 2.1. Materials and electrolysis cell

All experiments were performed in a rectangular glass cell ($20 \times 5 \times 5$ cm) described previously [39]. A schematic including the camera configuration (see below) is shown in the SI in figure S1. As electrolyte, 200 ml of 0.01 M KOH were used. The electrolyte solution was prepared from KOH pellets ($\geqslant 85\%$, Carl Roth) and deionized water ($\leqslant 700\,\mu S\,cm^{-1}$). The Au wire electrode (purity at least 99.99%) with a diameter of 0.5 mm was purchased from MaTecK. Before each experiment, the electrode was annealed for 3 min in a propane torch (CAMPINGAZ) to remove organic contaminations and flatten the electrode surface. Electrode holders were 3D-printed using chemically resistant PVDF purchased from 3Dogg.

### 2.2. Electrolysis

In all experiments, a voltage of 300 V was applied with a Magpuls MP2-30 power supply using the Au wire as the cathode and a stainless steel block ($2 \times 0.4 \times 2$ cm) as the anode.

Voltage and current were measured using a digital oscilloscope (WaveRunner 8254 2.5 GHz, Teledyne LeCroy). The voltage was applied for around 100 s, during which the temperature of the electrolyte increased, leading to higher current densities over time (see section S2 in the SI). The experiment was then repeated in the heated electrolyte and with the electrodes in the same positions. Higher electrolyte temperatures have no measurable effect on the evolution of currents around plasma ignition. However, the ignition occurs earlier, as shown and discussed in section S2 in the SI. The data presented in this work, exemplifying our approach, is from a second electrolysis cycle, where the electrolyte temperature is about 50 °C. A second data set supporting our data was recorded with the same experimental setup. However, images showing individual discharges were not recorded 1 s, but 1 min after ignition. The images in that video are less sharp. Overall, similar conclusions can be drawn from the results. The dataset and the subtle differences are shown in the Supporting Information.

### 2.3. High-speed imaging

High-speed videos were recorded using a Vision Research Phantom VEO 410 L 1MP camera. In all experiments, the camera was located on the side of the cell, i.e. with the line of sight perpendicular to the line between the electrodes (see figure S1 in the SI) For imaging the ignition process and the stable vapor layer, a frame rate of 1000 fps, an exposure time of 50 $\mu$s and a resolution of 1280 × 800 pixels were chosen. Both the ignition process and the vapor layer were imaged during the same experiment, where a small ring light was used for background illumination. For imaging the individual discharges, a frame rate of 57 000 fps, an exposure time of 17 $\mu$s, and a resolution of 256 × 256 were chosen.

## 3. Results

### 3.1. Ignition process

The vapor formation and the subsequent ignition of the plasma were studied at a Au wire cathode by recording simultaneously the evolution of the current (sample interval of 1 ms) and taking images of the working electrode with a high-speed camera (1000 fps, with background illumination). The electrodes were immersed in a 0.01 M KOH solution (about 50 °C, see experimental section), and a voltage of 300 V was applied between the working electrode and the stainless steel counter electrode. The evolution of the current (blue, orange, and violet curve) during plasma ignition is shown in figure 1(a) along with the measured voltage (black). Figures 1(b)–(g) provide selected images of the system at different times along the current trace. The complete series of images (video) can be found in the Data Repository [40]. For the following discussion, we set the time $t_0 = 0$ to the point where there is no evident contact between the electrode and the electrolyte anymore (see below).

The measured voltage deviates slightly from the applied 300 V. A direct correlation between these changes and the effects observed in the camera images can not be drawn. In contrast, a qualitative correlation can be drawn between the evolution of the current and the images. For further discussion, we separate the time around the plasma ignition into three regions: (i) the pre-ignition region I (blue), (ii) the ignition region II (orange), and (iii) the continuous CGDE region III (purple). In the pre-ignition region I, the current fluctuates strongly. By qualitatively correlating the current fluctuations with the images, the fluctuations appear to be related to the dynamic formation and subsequent collapse of the vapor layer covering the entire electrode. For example, in figure 1(b) the vapor layer collapsed and the current shows a local maximum. Subsequently, the newly formed small bubbles close to the electrode move away from the electrode and coalesce into larger volumes of gas, and contact between the electrode and the electrolyte is established again. The transition from the formation of individual bubbles to the formation of a continuous vapor layer has been described as a result of hydrodynamic instabilities [28, 31]. A more detailed description of the bubble coalescence can be found in section S3 of the SI. Locally, the vapor layer around the electrode can extend several mm into the electrolyte, as illustrated in figure 1(c). For such extensive vapor layers, the contact area between the electrode and electrolyte decreases, leading to an increase in resistance at the interface. Consequently, the current reaches a local minimum.

When the gas film collapses (see figure 1(d)), the situation is similar to that in figure 1(b), where the electrode–electrolyte contact area increases, lowering the interfacial resistance, and leading to higher currents. This oscillating behavior of the current in region I occurs with a frequency of approximately 100 Hz. In the pre-ignition region I from about −117 to 0 ms, individual bright discharges are apparent at the tip of the electrode, marked by the white arrow in figure 1(c). This agrees with other studies that illustrated a higher probability for discharge formation on highly curved surfaces, e.g. edges, due to larger electric fields [36, 37].

Typically, these sparks are apparent from a purple emission by visual inspection. The color of the emission depends on the species present in the plasma, where, in this case, the dominant emission originates from K atoms [23]. In some images, such as in figure 1(c), also broader, less intense light spots are apparent within the thick vapor layer at different positions along the wire, as marked by the yellow arrow. We assume that the refraction of the background light most likely causes these features and is not related to the emission from discharges in this region of the vapor layer.

At the beginning of the ignition region II, the current fluctuations become less pronounced (0 ms in figure 1(a)). Here, a large bubble expands from the electrode tip along the entire electrode, which collapses to form a vapor layer around the electrode. Concomitantly, a discharge is observed at the electrode tip (see figure 1(e)), which appears to travel upwards along the wire. Since the electrode is no longer in contact with the electrolyte, the current is low in this region II. In the following frames after the ignition, individual bright discharges are

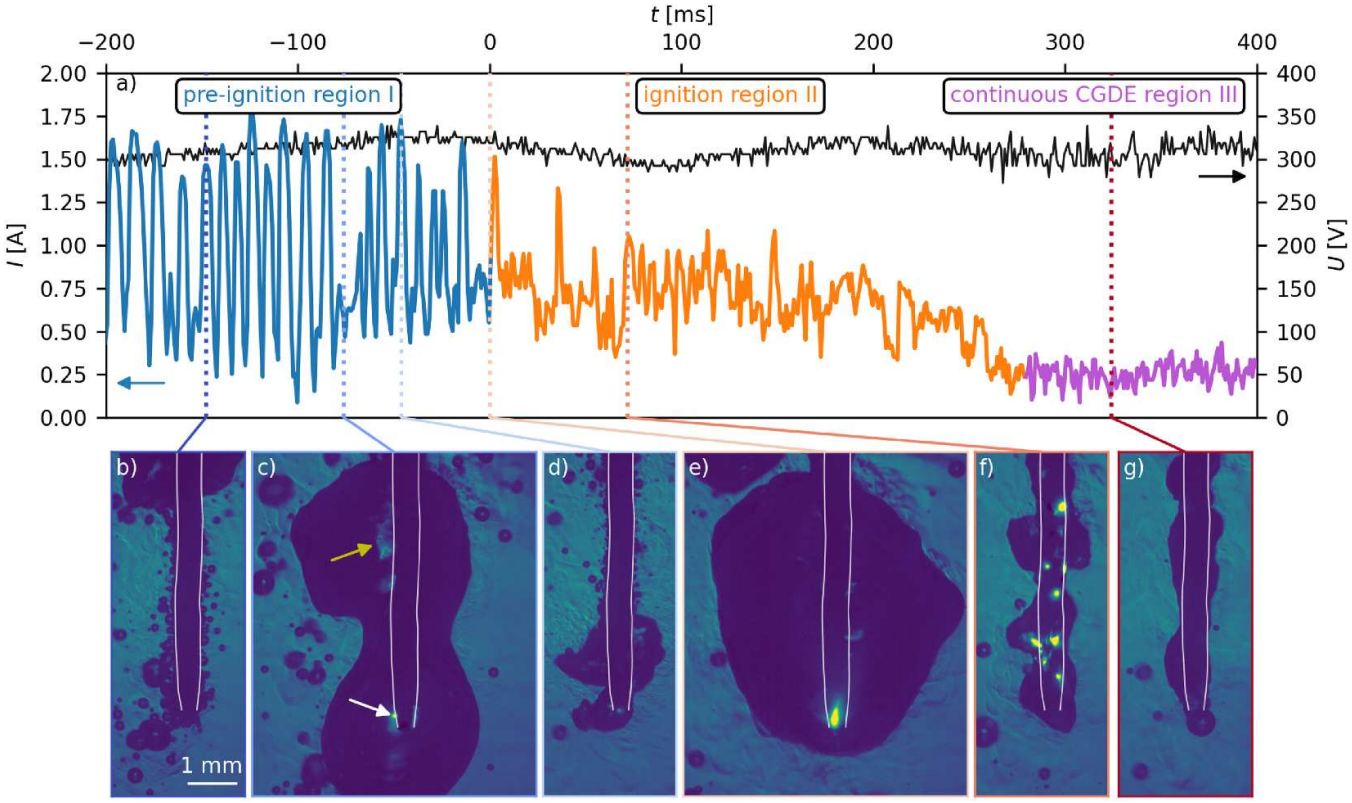


**Figure 1.** (a) Current (blue, orange, and violet) and voltage trace during the ignition process of CGDE with a voltage of 300 V and (b)–(g) high-speed camera images at times indicated by the dotted lines in the current trace. All images use the scale indicated in panel b. Ignition occurs at 0 ms. The border of the electrode is indicated in all images with white lines. The arrows in panel c indicate a supposed discharge (white) and reflection of the background light (yellow), as explained in the text.

observed, as illustrated in figure 1(f). Approximately 280 ms after the ignition, continuous CGDE is observed in region III, apparent by a decrease in discharge intensity and less pronounced fluctuations in the current. These fluctuations do not change significantly for longer time scales, as shown in the SI in figure S2 (constant for at least 1 min, i.e. the rest of the experiment). These small current fluctuations indicate that the electrode is completely isolated from the electrolyte by a comparably stable vapor layer. The discharges can no longer be discerned from the refraction of the background light. However, the purple emission remains evident to the eye as a continuous purple glow. The camera images recorded without background illumination (see figure 3 below) clearly show that the glow results from individual discharges in this region III. We suggest that the change from high-intensity discharges that contribute significantly to the current in region II to stable lower-intensity discharges in region III is related to a change in the discharge mechanism in both regions. A more detailed study on the ignition process should be addressed in a separate work. In the following, we focus on the vapor layer thickness and discharges in region III during continuous CGDE.

### 3.2. Vapor layer thickness

In the CGDE region III, the current density is almost constant, and the vapor layer does not change significantly compared to regions I and II, allowing for a more quantitative evaluation of the processes. We determined the average size of the vapor layer from the high-speed camera images recorded in this region III. A dataset of 740 images, recorded with a frame rate of 1000 fps and starting at 460 ms after the ignition, was used for the analysis. In each image 600 rows of pixels were evaluated, which includes almost the entire wire (excluding the tip of the wire and the region close to the electrolyte surface). The documentation on the underlying Python-based custom tools can be found in the supporting material and reference [40]. The evaluation of each frame is illustrated for a representative image depicted in figure 2(a). The outline of the electrode, determined from an image before the electrolysis, is indicated by dotted white lines and the center of the wire by a solid gray line. The border between the vapor layer and the electrolyte was determined for each line in the image on each electrode side by detecting steps in the pixel brightness and is indicated by the solid white line in figure 2(a). In some regions of the images, artifacts are observed (marked by a yellow circle), which are primarily caused by changes in the refractive index in the proximity of the vapor layer. This phenomenon is also known as schlieren. The frequency of these artifacts is, however, low and is not significant for the following statistical evaluation. The region around the electrode tip was not considered in the analysis due to the more complex convex shape of the vapor layer there.

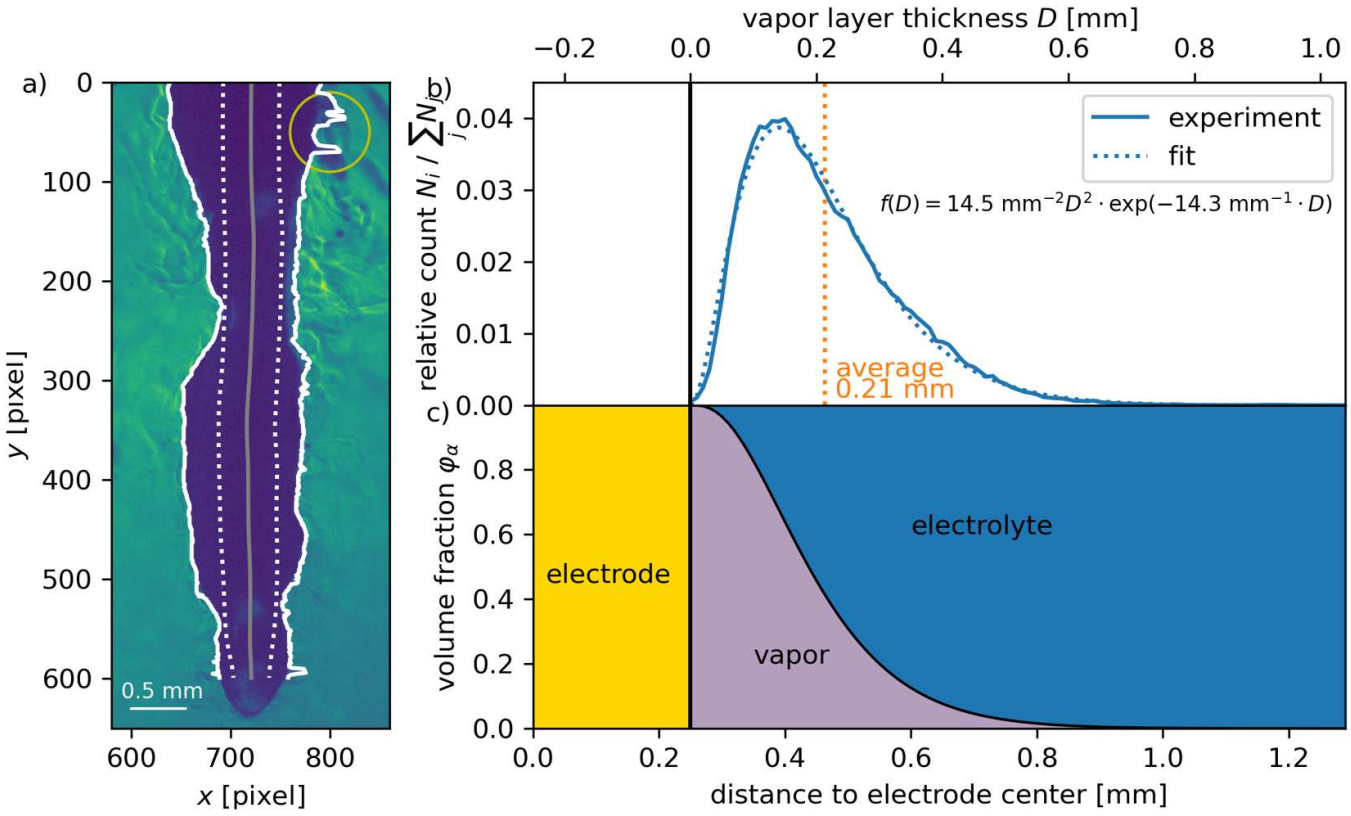


**Figure 2.** (a) Image of the vapor layer surrounding the working electrode taken with background illumination at $t = 526\,\mathrm{ms}$ after ignition. The edges of the electrode (dotted) as well as the border between the vapor layer and the electrolyte (solid) are indicated as white lines. The center of the electrode is indicated by a solid gray line. (b) Normalized histogram of the vapor layer thickness over 740 frames during CGDE with a Au cathode at 300 V. The experimental data with a bin size of 0.01 mm is shown as a solid blue line and the fitted distribution is shown as a dotted blue line. The average thickness is indicated by a dotted orange line. (c) The contribution of each phase with increasing distance from the working electrode center is obtained by integrating the distribution in (b). Displayed are the volume fractions of each phase (electrode, vapor, and electrolyte), i.e. the probabilities of their presence at a certain distance to the electrode center.

The vapor layer thickness $D$, i.e. the distance between the electrode and the vapor–electrolyte interface, was determined line by line for all vertical positions on either side of the electrode in all frames. First, we show in figure S4 that the average vapor layer thickness along the wire increases from the tip upwards to the electrolyte surface (average thickness at the bottom is 0.15 mm and at the top 0.3 mm). The distribution is similar on either side of the electrode. This increase in vapor-layer thickness can be rationalized by the buoyancy of the gas produced mainly by electrolyte evaporation, as explained in the SI in section S4. There is no significant difference in vapor-layer thickness between the side close to the counter electrode (right) and the opposing side (left), indicating that the electrode arrangement does not affect this property.

The vapor layer thickness distribution, including all thicknesses along the wire, is shown in figure 2(b) by the solid blue line (bin size of 0.01 mm). The most frequent thickness is 0.15 mm, while the average thickness is 0.21 mm. The maximum thickness is around 0.7 mm. The distribution can be fitted using an empirical equation with a quadratic and an exponential component:

$$f(D) = AD^2 \mathrm{e}^{-BD}, \tag{1}$$

where $f(D)$ represents the count of occurrence of the vapor layer thickness $D$, with $A$ and $B$ being fitting parameters. While equation (1) does not necessarily have a direct physical origin, it is relevant for further evaluation below. The fitted distribution (using parameters $A = 14.5\,\mathrm{mm}^{-2}$ and $B = 14.3\,\mathrm{mm}^{-1}$) is shown by the dotted blue line in figure 2(b).

From this fit, one can now infer the probability of finding the vapor–electrolyte interface at a distance $D_x$ from the electrode by integrating the fitted distribution in an interval between $D = 0$ and $D = D_x$, and normalizing it by the total integral. The probability of finding a phase $\alpha$ (vapor or electrolyte) at a certain distance from the electrode equals the volume fraction $\varphi_\alpha$ averaged over all positions with that distance to the electrode. The volume fraction of the electrolyte $\varphi_{\mathrm{el}}$ can be expressed by integrating equation (1),

$$\begin{aligned}\varphi_{\mathrm{el}}(D_x) &= \frac{V_{\mathrm{el}}}{V}(D_x) = \frac{\int_0^{D_x} f(D)\,\mathrm{d}D}{\int_0^{\infty} f(D)\,\mathrm{d}D} \\ &= \frac{1}{2}\left(\mathrm{e}^{-BD_x}\left(-BD_x(BD_x+2)-2\right)+2\right). \end{aligned} \tag{2}$$

The integrated distribution of the volume fraction is shown in figure 2(c). The $x$-axis is now presented as the distance to the electrode center to include the solid phase. On the electrode

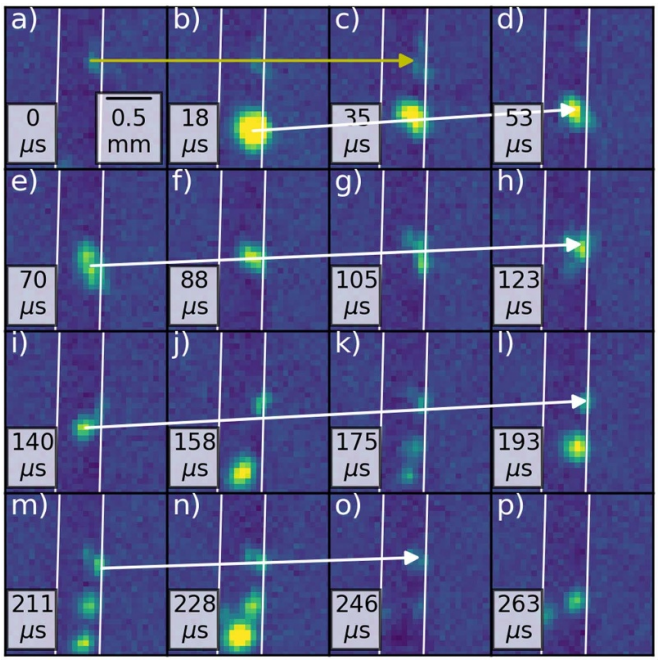


**Figure 3.** Consecutive high-speed camera images of the electrode about one second after the plasma ignition. The time relative to image a is given in the lower left corner of each image. The white arrow shows a discharge that moves slightly upward and the yellow arrow a discharge that remains almost at the same position.

surface (0.25 mm from the electrode center), the probability for the occurrence of the vapor phase is 100%. With increasing distance from the electrode surface, the vapor volume fraction decreases. At a distance of approximately 0.45 mm to the electrode center, liquid and vapor phases are equally likely. At 0.65 mm and beyond, the electrolyte phase dominates. Further below, we show how the vapor layer thickness can also be inferred from the analysis of discharges. The obtained distribution can be used for a more detailed plasma-physics analysis of the discharges, which is beyond the scope of this work.

### 3.3. *Individual discharges—qualitative*

As described above, during continuous CGDE, a glow is apparent by the naked eye, while discharges were not observed in the camera images using background illumination (see figure 1(f)). Performing a similar experiment but without background illumination (with a much higher frame rate of 57 000 fps, i.e. image interval of 17 $\mu$s) reveals individual discharges at different positions on the wire, which are apparent from the video provided in the Data Repository [40] and illustrated for a selected series of consecutive images in figure 3 (ca. 1 s after ignition). Note that these images and those further below have been post-processed to remove image artifacts, such as streaks of bright pixels due to the low exposure times, located at identical positions throughout the videos. The images show the same region located approximately in the middle of the lower half of the wire. The observation of individual discharges has been reported previously for rod electrodes and was suggested to occur when the plasma is only partially ignited [35].

Qualitatively, we can deduce the formation of single discharges and their movement along the wire surface within the vapor layer from the images in figure 3. Most discharges are present only for one or two frames. Figure S5 shows the distribution of discharge lifetimes, where most discharges have a lifetime lower than 100 $\mu$s. Discharges can move in all directions, both vertically and horizontally. One example where a discharge stays in the same position for a few frames is indicated in figures 3(a)–(c) with a yellow arrow. In figure 3(b), a new discharge appears, which was not observed in the previous frame. In this case, the emission is brightest in this first frame and decreases in the following 200 $\mu$s until the discharge disappears (white arrow). Initially, it is located in a fairly central image area, moving toward the edge of the wire in the following frames. Note that, in principle, it is impossible to infer from our measurements whether discharges extinguish or move to a position at the back of the wire. Still, movement to the back side is also not unlikely, as shown in figure S6. Further, quantitative information on the discharge movement is given below.

### 3.4. *Individual discharges—quantitative*

To gain more quantitative insights into the location, brightness, mobility, and shape of the discharges, we created a Python-based toolbox that extracts these parameters for each discharge for each frame. For the following results, we use a dataset consisting of 6000 frames and ca. 55 000 discharge spots. Note that the number of distinct discharges is lower since they appear as individual spots in consecutive images (see discharges followed by arrows in figure 3). The code for extracting the individual discharge spots from its local brightness in the image can be found in the supporting material and reference [40]. In the following, we only focus on the conceptual ideas and the results.

*3.4.1. Current correlation.* In regions I and II, we correlated the fluctuations in the current with the dynamic formation and collapse of the electrode–electrolyte interface, where higher currents are observed when the electrode is in contact with the electrolyte. In region III, the fluctuation in the current is comparably smaller (see figure 1). Nevertheless, fluctuations are still observed, as shown in figure 4 (blue trace), which can not simply be related to changes in the vapor layer thickness from comparing individual images. Considering that the vapor layer has a negligible conductivity, all current must pass through the discharges, and the current correlates with their intensity, which was suggested previously [35]. Thus, one would expect the current to be larger for times with stronger total emission. Note that the total intensity is, in the case of predominantly line radiation, linearly proportional to the electron density and shows exponential dependence on the electron temperature or mean electron energy. Hence, an increased current partly corresponds to an increased emission. In the case of a constant electron energy distribution function, the correlation between the current and the emission is clear. Camera images recorded along with the current for a region with high and low intensity are provided in the figure, from which such correlations can

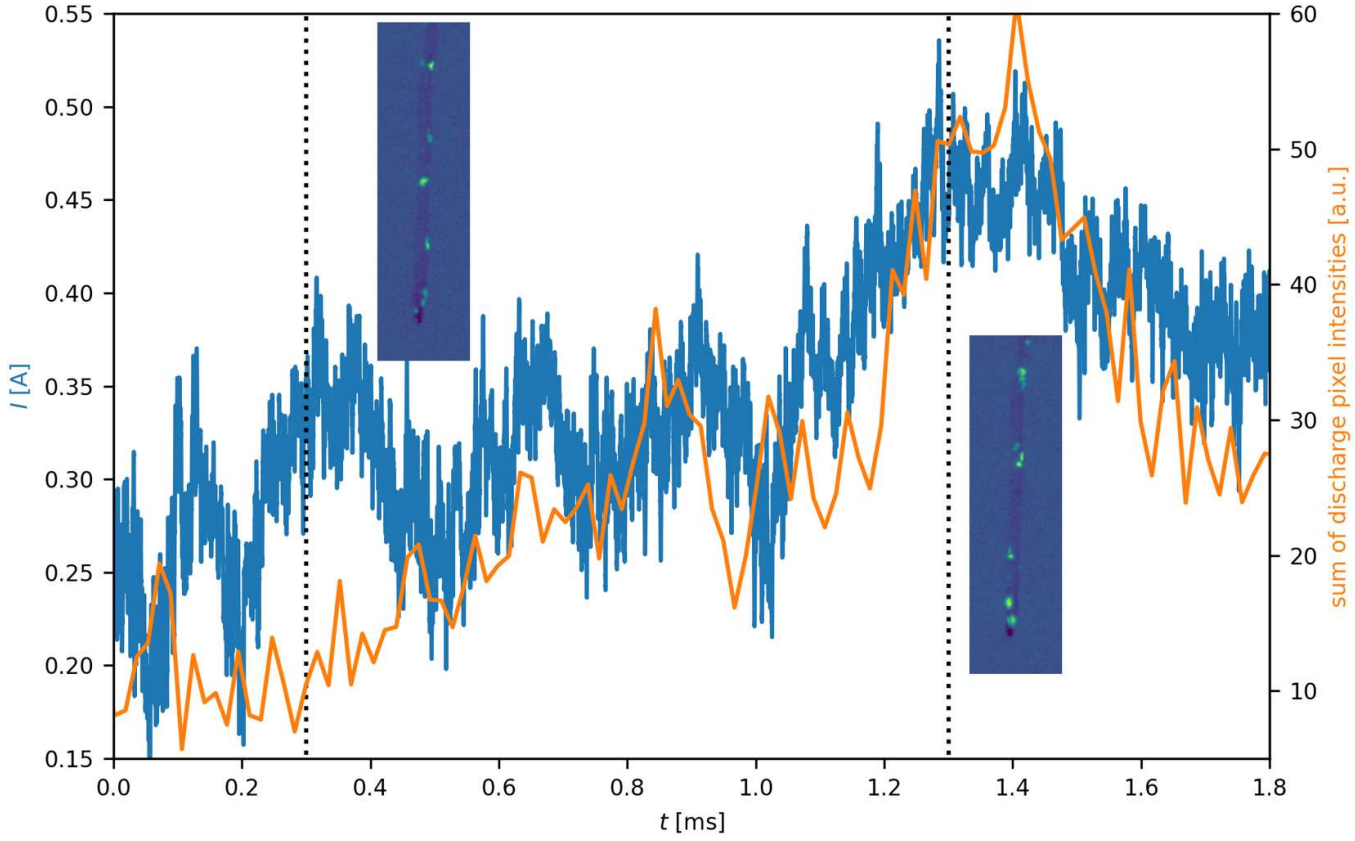


**Figure 4.** Comparison between the current (blue) and the total discharge intensity of each frame (orange). The latter was obtained by summing all pixel intensities above a certain threshold for each of the 102 frames shown (1.8 ms) during CGDE with a Au cathode at 300 V. For comparison, pictures of the discharges at 0.3 and 1.3 ms are included.

hardly be drawn from visual inspection. Therefore, we determined for each image the total intensity of plasma emission by summing up the intensity of each discharge pixel above a certain threshold, shown by the orange trace. A match between the intensity and current profile seems only valid for the region of $t > 0.8$ ms, in contrast to the region of $t < 0.8$ ms. The discrepancy in this regime is most likely due to geometric constraints. When most of the discharges are located in front of the wire (and almost no discharges would be present on the back side of the wire), there is good agreement. On the other hand, discharges behind the wire are obscured and contribute to the current without being detected by the camera. We assume this is the case in the region of $t < 0.8$ ms.

From the qualitative description of the discharges in the video, it was apparent that the discharges seemed to move upwards, while from the individual images, such a movement was not so clear (some discharges remained in the same vertical position, while others moved slightly upwards). Considering that the vapor layer thickness increases from the bottom of the wire to the electrolyte surface (see above), we determined the vertical distribution of the discharges along the wire, shown in figure S7 in the SI. It is apparent that the frequency of discharges is highest around the tip but is similar for all other positions along the wire. The higher number of discharges at the tip is likely due to the high electric fields at this position rather than the thickness of the vapor layer [33–37]. Based on this result, the apparent upward motion in the video can only be explained by the formation of discharges at the tip, which move upward, where some discharges extinguish slightly above the wire tip. Then, the number of discharges remains constant.

Detailed insights are gained from taking a more careful look at a series of images from the video shown in section S8 of the SI. Here, an inhomogeneous distribution of discharges along the wire is observed, with regions of lower and higher discharge density (discharge agglomerates). A similar phenomenon was reported elsewhere for planar electrodes [24]. From subsequent images of the discharges, we determined the velocity of individual discharges and that of discharge agglomerates (see section S8 in the SI). The velocity distribution of individual discharges suggests a net velocity of zero in either direction (figure S8(e)) and, hence, can not be at the origin of the observed upward motion of the discharges. However, the mean group speed of all discharges (or discharge agglomerates) is about 0.19 m $s^{-1}$ (0.22 m $s^{-1}$ for the second data set) in an upward direction (see also figure S8(d)). To gain more definite values including error bars larger data sets are required. This means that the upward movement of discharge groups is not a combination of many upward-moving individual discharges. Rather, discharges at the lower part of the

group extinguish, and new discharges ignite at the upper part of the group. The effect of the preferred ignition of discharges in the vicinity of a group of discharges was observed elsewhere on planar electrodes [24]. A possible explanation could be that hot gas ascends, and with it potentially ions or other species which could enable easier re-ignition, similar to a gliding arc discharge, sometimes denoted as 'Jacob's ladder' [41, 42].

Next, we focus on the size and shape of the individual discharges observed in each image. An example image is given in figure 5(a). In comparison, figure 5(b) shows a schematic illustration of the wire, the vapor layer, the electrolyte, and discharges with different shapes and at different locations. For the discharges, we assume a spheroid shape, which can be either oblate or prolate depending on the ratio of vapor layer thickness and the lateral diameter of the discharges. In the 2-dimensional camera images, the observed shape depends on the position of the discharge on the wire. A discharge located at the center of the wire appears circular (D1 in figure 5(b)). For the discharges at the edge of the wire (D2 and D3), the vertical length of the discharge image corresponds to its lateral diameter. In contrast, the horizontal length corresponds to the vapor layer thickness. The 2-dimensional shape is, in both cases, an ellipse, with the major axis parallel (D1) or perpendicular (D2) to the wire surface. Thus, in the following we distinguish between the discharges based on their position, i.e. center and edge discharges. This separation allows the size of the discharges in all three dimensions to be determined.

For each discharge spot, an ellipse was fitted to the discharge border, as illustrated in figure 5(c). This yields the ellipse height $h$, i.e. the length of the major axis (green line), the ellipse width $w$, i.e. the length of the minor axis (orange line), and the angle $\gamma$ between the major axis and the $y$-axis. The major axis is parallel to the wire for $\gamma = 0°$ and perpendicular for 90°. For the following analysis, discharges smaller than two pixels were omitted.

Figure 5(d) shows the fit data for all discharge spots, where the angle $\gamma$ is plotted vs. the horizontal position of the ellipse (spot) center relative to the wire center. For our electrode with a diameter of 0.5 mm the edges are located at $\pm 0.25$ mm (dashed line). For further discussion, we denote the area at $\pm 0.125$ mm (dotted line) as the central region.

The color of each point indicates the ratio between the spot width and spot height ($w/h$), i.e. the circularity of the ellipse. Yellow spots mark near-perfect circles where both ellipse axes have a similar length. The violet spots represent ellipses where one axis is significantly longer than the other. For better visibility, spots with high ($w/h > 0.7$) and low ($w/h < 0.7$) circularities are shown separately in figure S9 in the SI. In the central region, the ellipses do not have a preferred angle, and the discharge spots are mostly circular. In contrast, the spots at the edges appear mostly as ellipses (violet color), which are predominantly oriented parallel to the wire surface ($\gamma = 0°$, green region in the figure). Less frequent but still dominant are ellipses with an angle $\gamma = \pm 90°$ at the upper and lower

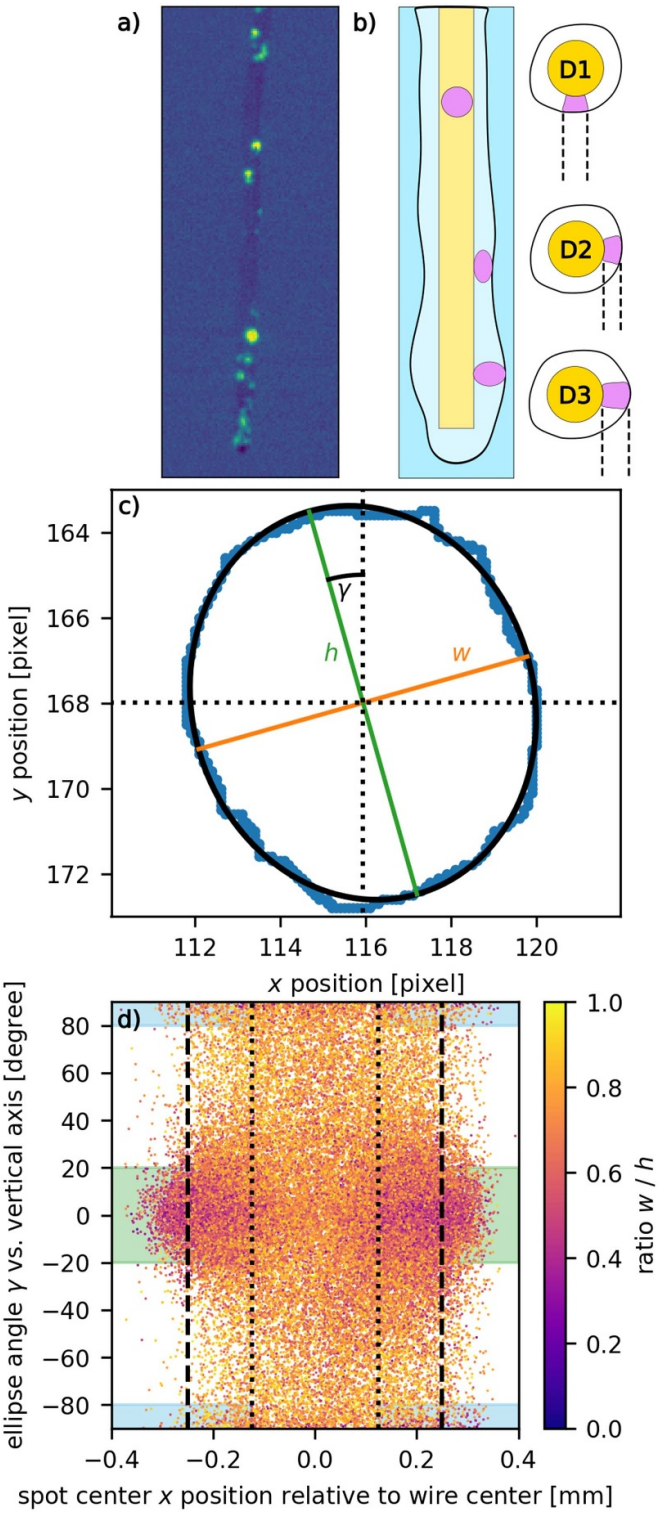


**Figure 5.** (a) Image of the wire 1 s after ignition without background illumination (b) Scheme of discharges within the vapor layer. D1: Discharge at the wire center. D2: Oblate discharge at the wire edge. D3: Prolate discharge at the wire edge. (c) Elliptical fit of a single discharge. (d) Separation of discharges into circular spots in the center and elliptical fits at the edge. The electrode border is indicated by the dashed lines and the border between center and edge positions by the dotted lines.

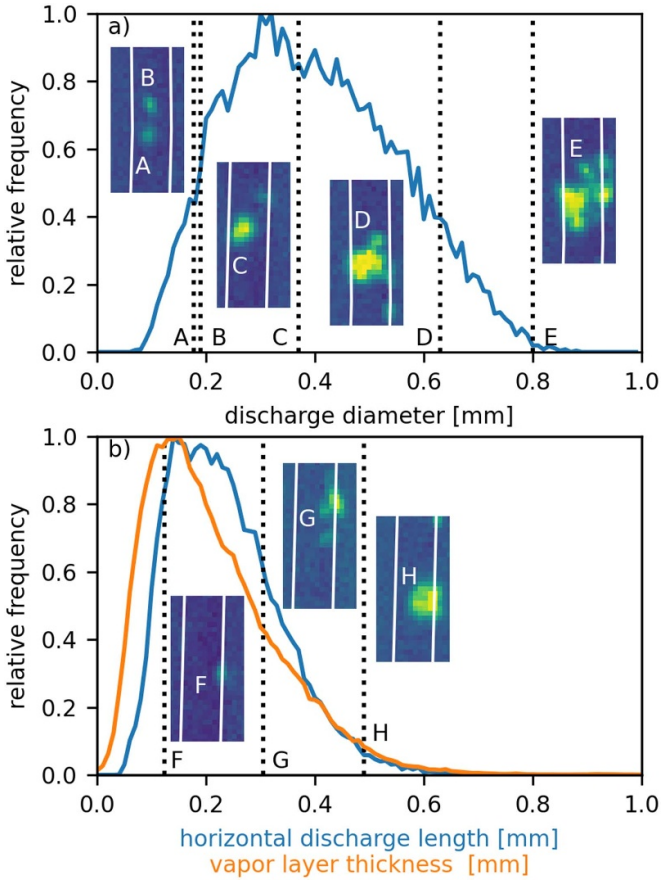


**Figure 6.** (a) Histogram of discharge diameters for discharges in the central area. The discharge diameter was determined as the average of both axes of the fitted ellipse. (b) Histogram of horizontal discharge lengths (blue) of discharges at the edge of the wire. For comparison, the histogram for the vapor layer thickness from figure 2 is also included (orange). In both graphs, example images of discharges are included, and dashed lines mark their location in the diagram. In the images, the electrode outline is indicated by a white line. For all distributions, the bin size is 0.01 mm.

part of the figure (blue regions), hence, oriented perpendicular to the surface. From this analysis, we separate all discharges into two groups: (i) discharges in the center of the wire, which appear mostly circular and (ii) discharges at the edge of the wire, appearing as ellipses. Different information can be obtained from the discharges within each of these groups.

The circular discharges in the center (for group (i)) provide information on the cross-section of the discharges through which the current flows. Figure 6(a) shows a histogram of discharge sizes in this region. Representative images of selected discharges are included in the figure, where the labels relate to those marking the vertical lines in the plot. The discharge diameter was determined from the average length of both ellipse axes. The distribution has a maximum at around 0.3 mm. Discharges located at around the maximum and below, with small diameters (<0.4 mm), are mostly confined to the central area of the wire (spots A to C). Larger spots can have diameters larger than that of the wire (spot D). Discharge spots with a size significantly larger than the wire (about 0.8 mm, spot E) seem to consist of multiple overlapping spots that can not be separated with our evaluation and the resolution of the recorded images (see also figure S6).

The ellipsoidal discharges located at the edge of the wire, i.e. where the center of the ellipse is located outside of the wire diameter, primarily provide information on the vapor layer thickness, assuming that the discharge stretches from the electrode to the electrolyte. The horizontal width of each edge discharge spot was determined by the difference in the $x$-coordinate of the left- and rightmost pixels of the fitted ellipses. Figure 6(b) shows in blue a histogram of the horizontal width of these discharges in comparison to the histogram of the vapor layer thickness deduced from the videos recorded with background illumination in orange (same data as in figure 2(a)). The distribution of the vapor layer thickness deduced from the shape of the discharges (blue) shows a maximum just below 0.2 mm. At small discharge lengths/thicknesses small deviations originate from the evaluation, where spots with sizes smaller than two pixels (0.125 mm) were omitted. The distribution of discharge widths is skewed somewhat towards larger distances compared to the vapor layer thickness in the region of intermediate widths (0.2–0.4 mm). The shift could be caused by discharges located between the edge discharges and the the center discharges, where the center of the ellipse is located outside of the wire perimeter, but the lateral extent still overlaps with the wire. Many of the largest discharges, such as spot H in figure 6(b), extend to positions far away from the wire edge, which is most likely caused by a discharge with a large diameter wrapping around to the front of the wire. Overall, the distribution is narrower than for the discharges in the center in figure 6(a). This means the discharges parallel to the electrode surface are larger than those perpendicular to it, i.e. the discharges are predominantly oblate spheroids (D2 in figure 5). Most importantly, the distributions of the width of edge discharges correlate nicely with the thickness of the vapor layer.

In conclusion, the detailed analysis of discharge spots recorded by a high-speed camera reveals the shape and size distribution of these discharges in three dimensions. This is possible from two-dimensional images due to the electrode's curvature and the resulting viewing angle between the discharge and the camera. In general, the discharges have the shape of spheroids, which are mostly oblate (where the length perpendicular to the surface is smaller than the diameter parallel to the electrode surface). However, some prolate spheroids are also present.

## 4. Conclusion

In this work, we studied the vapor layer engulfing the working electrode during CGDE at 300 V with a Au wire cathode using high-speed camera imaging. From quantitative comparisons

and detailed statistical analysis of the vapor layer and the discharges within, we derived the following aspects:

- Before the plasma ignition the current fluctuated strongly, which was related to the formation and collapse of the electric contact between the electrode and electrolyte.
- The plasma finally ignites with a strong discharge at the wire tip within a large bubble, which expands over the entire electrode, followed by forming a stable vapor layer and continuous plasma after about 300 ms.
- The discharges in the ignition region are apparent from camera images using background illumination, while those during CGDE (visible by the naked eye) are not visible, indicating a difference in their discharge properties or mechanism.
- The high-speed camera videos suggested an upward movement of discharges, which was based on statistical analysis, rationalized by the extinction of discharges at the lower part of discharge agglomerates on the wire and the ignition of new discharges at the top of these agglomerates. The net average velocity of individual discharges was found to be zero.
- The individual discharges were fitted assuming a spheroid structure, and were separated into two groups according to their shape and position. Spots in the center appear circular, while those on the wire edge appear as ellipses, suggesting that the discharges have an oblate spheroid shape.
- The distribution of the lengths of the discharges perpendicular to the electrode surface agrees well with the vapor layer thickness deduced separately, illustrating that the discharge extends from the electrode surface to the vapor–electrolyte interface, and suggests that discharges are equally likely to ignite anywhere on the wire independent from the vapor layer thickness.

In total, statistical analysis of the temporal evolution of high-speed camera imaging can provide insightful information on the fundamental properties of plasmas formed at electrodes in a solution. The applicability of our statistical analysis is possibly not limited to wire electrodes, but we expect it to be easily adaptable to other electrodes or plasma processes, such as plasma electrolytic oxidation.

Furthermore, we are confident that in combination with other characterization techniques, the fundamental understanding of local processes during CGDE might become available, i.e. related to electrode surface modification, such as nanoparticle formation, the formation mechanism and properties of individual discharges, and the reactions occurring at the discharge-electrolyte interface or in the electrolyte solution.

## Data availability statement

All data that support the findings of this study are included within the article (and any supplementary files).

## Acknowledgment

The authors gratefully acknowledge support from the DFG (German research foundation) through the collaborative research center CRC1316 (Project 327886311).

## CRediT

**L. Forschner**: Conceptualization, Formal Analysis, Investigation, Validation, Visualization, Writing—Original Draft Preparation. **J.-L. Gembus**: Investigation, Writing—Review & Editing. **L. Schücke**: Supervision, Writing—Review & Editing. **P. Awakowicz**: Funding Acquisition, Resources, Supervision, Writing—Review & Editing. **A.R. Gibson**: Funding Acquisition, Resources, Supervision, Writing—Review & Editing. **T. Jacob**: Funding Acquisition, Resources, Supervision, Writing—Review & Editing. **A. K. Engstfeld**: Funding Acquisition, Conceptualization, Supervision, Writing—Review & Editing

## ORCID iDs

Lukas Forschner https://orcid.org/0000-0002-1551-5045
Jan-Luca Gembus https://orcid.org/0009-0002-1263-9218
Lars Schücke https://orcid.org/0000-0002-7991-853X
Peter Awakowicz https://orcid.org/0000-0002-8630-9900
Andrew R Gibson https://orcid.org/0000-0002-1082-4359
Timo Jacob https://orcid.org/0000-0001-7777-2306
Albert K Engstfeld https://orcid.org/0000-0002-9686-3948

## References

[1] Fizeau H and Foucault L 1844 Recherches sur l'intensite de la lumiere emise par le charbon dans l'experience de Davy *Ann. Chim. Phys.* **11** 370–84 (available at: https://mdz-nbn-resolving.de/details:bsb10071785)
[2] van der Willigen V S M 1856 Ueber Licht- und Wärme-Erscheinungen bei einer kräftigen galvanischen Batterie; Bildung des Lichtbogens zwischen Metall und Flüssigkeit, und Auftreten von Licht an einer der in die Flüssigkeit getauchten Elektroden *Ann. Phys.* **169** 285–96
[3] Kellogg H H 1950 Anode effect in aqueos electrolysis *J. Electrochem. Soc.* **97** 133–42
[4] Hickling A and Ingram M D 1964 Contact glow-discharge electrolysis *Trans. Faraday Soc.* **60** 783–93
[5] Saito G, Akiyama T and Chen W 2015 Nanomaterial synthesis using plasma generation in liquid *J. Nanomater.* **2015** 123696
[6] Horikoshi S and Serpone N 2017 In-liquid plasma: a novel tool in the fabrication of nanomaterials and in the treatment of wastewaters *RCS Adv.* **7** 47196–218
[7] Bruggeman P J *et al* 2021 Plasma-driven solution electrolysis *J. Appl. Phys.* **129** 200902
[8] Adamovich I *et al* 2022 The 2022 plasma roadmap: low temperature plasma science and technology *J. Phys. D: Appl. Phys.* **55** 373001
[9] Hickling A, Newns G R 1961 Glow-discharge electrolysis. Part V. The contact glow-discharge electrolysis of liquid ammonia *J. Chem. Soc.* 5186–91

[10] Harada K and Iwasaki T 1974 Syntheses of amino acids from aliphatic carboxylic acid by glow discharge electrolysis *Nature* **250** 426–8
[11] Malik M A, Ghaffar A and Malik S A 2001 Water purification by electrical discharges *Plasma Sources Sci. Technol.* **10** 82–91
[12] Wang X, Zhou M and Jin X 2012 Application of glow discharge plasma for wastewater treatment *Electrochim. Acta* **83** 501–12
[13] Sengupta S K 2017 Contact glow discharge electrolysis: a novel tool for manifold applications *Plasma Chem. Plasma Process.* **37** 897–945
[14] Yerokhin A L, Nie X, Leyland A, Matthews A and Dowey S J 1999 Plasma electrolysis for surface engineering *Surf. Coat. Technol.* **122** 73–93
[15] Paulmier T, Bell J M and Fredericks P M 2007 Development of a novel cathodic plasma/electrolytic deposition technique part 1: production of titanium dioxide coatings *Surf. Coat. Technol.* **201** 8761–70
[16] Artmann E, Forschner L, Schüttler K M, Al-Shakran M, Jacob T and Engstfeld A K 2022 Nanoporous Au formation on Au substrates via high voltage electrolysis *ChemPhysChem* **24** e202200645
[17] Zheng B, Wang K, Shrestha M, Schuelke T and Fan Q H 2019 Understanding the chemical reactions in cathodic plasma electrolysis *Plasma Sources Sci. Technol.* **28** 085016
[18] Kareem T A and Kaliani A A 2012 Glow discharge plasma electrolysis for nanoparticles synthesis *Ionics* **18** 315–27
[19] Allagui A, Baranova E A and Wüthrich R 2013 Synthesis of Ni and Pt nanomaterials by cathodic contact glow discharge electrolysis in acidic and alkaline media *Electrochim. Acta* **93** 137–42
[20] Sengupta S K and Singh O P 1994 Contact glow discharge electrolysis: a study of its chemical yields in aqueous inert–type electrolytes *J. Electroanal. Chem.* **369** 113–20
[21] Quanfang L, Jie Y, Jinzhang G and Wu Y 2005 Glow discharge induced hydroxyl radical degradation of 2-naphthylamine *Plasma Sci. Technol.* **7** 2856–9
[22] Artmann E, Menezes P V, Forschner L, Elnagar M M, Kibler L A, Jacob T and Engstfeld A K 2021 Structural evolution of Pt, Au and Cu anodes by electrolysis up to contact glow discharge electrolysis in alkaline electrolytes *ChemPhysChem* **22** 2429–41
[23] Azumi K, Mizuno T, Akimoto T and Ohmori T 1999 Light emission from Pt during high-voltage cathodic polarization *J. Electrochem. Soc.* **146** 3374–7
[24] Saito G, Nakasugi Y and Akiyama T 2014 High-speed camera observation of solution plasma during nanoparticles formation *Appl. Phys. Lett.* **104** 083104
[25] Vogt H and Balzer R J 2005 The bubble coverage of gas-evolving electrodes in stagnant electrolytes *Electrochim. Acta* **50** 2073–9
[26] Vogt H 2012 The actual current density of gas-evolving electrodes—notes on the bubble coverage *Electrochim. Acta* **78** 183–7
[27] Zhao X, Ren H and Luo L 2019 Gas bubbles in electrochemical gas evolution reactions *Langmuir* **35** 5392–408
[28] Mazza B, Pedeferri P and Re G 1978 Hydrodynamic instabilities in electrolytic gas evolution *Electrochim. Acta* **23** 87–93
[29] Wüthrich R, Comninellis C and Bleuler H 2005 Bubble evolution on vertical electrodes under extreme current densities *Electrochim. Acta* **50** 5242–6
[30] Allagui A and Wüthrich R 2009 Gas film formation time and gas film life time during electrochemical discharge phenomenon *Electrochim. Acta* **54** 5336–43
[31] Gangal U, Srivastava M and Gupta S K S 2009 Mechanism of the breakdown of normal electrolysis and the transition to contact glow discharge electrolysis *J. Electrochem. Soc.* **156** F131–6
[32] Vogt H and Thonstad J 2017 The diversity and causes of current-potential behaviour at gas-evolving electrodes *Electrochim. Acta* **250** 393–8
[33] Schaper L, Graham W G and Stalder K R 2011 Vapour layer formation by electrical discharges through electrically conducting liquids—modelling and experiment *Plasma Sources Sci. Technol.* **20** 034003
[34] Schaper L, Stalder K R and Graham W G 2011 Plasma production in electrically conducting liquids *Plasma Sources Sci. Technol.* **20** 034004
[35] Saito G, Nakasugi Y and Akiyama T 2014 Excitation temperature of a solution plasma during nanoparticle synthesis *J. Appl. Phys.* **116** 083301
[36] Stojadinović S, Jovović J, Tadić N, Vasilić R and Šišović N M 2015 The characterization of cathodic plasma electrolysis of tungsten by means of optical emission spectroscopy techniques *Europhys. Lett.* **110** 48004
[37] Yerokhin A, Mukaeva V R, Parfenov E V, Laugel N and Matthews A 2019 Charge transfer mechanisms underlying contact glow discharge electrolysis *Electrochim. Acta* **312** 441–56
[38] Van Rossum G and Drake F L 2009 *Python 3 Reference Manual* (CreateSpace) (https://doi.org/10.5555/1593511)
[39] Forschner L, Artmann E, Jacob T and Engstfeld A K 2023 Electric potential distribution inside the electrolyte during high voltage electrolysis *J. Phys. Chem. C* **127** 4387–94
[40] Forschner L*et al* 2025 DATASET: statistical analysis of the dynamic behavior of individual discharges during the ignition and continuous phases of contact glow discharge electrolysis *Zenodo* (https://doi.org/10.5281/zenodo.14775730)
[41] Czernichowski A 1994 Gliding arc. Applications to engineering and environment control *Pure Appl. Chem.* **66** 1301–10
[42] Kolev S and Bogaerts A 2015 A 2D model for a gliding arc discharge *Plasma Sources Sci. Technol.* **24** 015025